Electronic structure and bonding of the 3*d* transition metal borides, MB, M=Sc, Ti, V, Cr, Mn, Fe, Co, Ni, and Cu through all electron *ab initio* calculations

Demeter Tzeli[a] and Aristides Mavridis[b]
Laboratory of Physical Chemistry, Department of Chemistry, National and Kapodistrian University of Athens, P.O. Box 64 004, Zografou, Athens 157 10, Greece

(Received 24 September 2007; accepted 9 November 2007; published online 17 January 2008)

The electronic structure and bonding of the ground and some low-lying states of all first row transition metal borides (MB), ScB, TiB, VB, CrB, MnB, FeB, CoB, NiB, and CuB have been studied by multireference configuration interaction (MRCI) methods employing a correlation consistent basis set of quintuple cardinality (5Z). It should be stressed that for all the above nine molecules, experimental results are essentially absent, whereas with the exception of ScB and CuB the remaining seven species are studied theoretically for the first time. We have constructed full potential energy curves at the MRCI/5Z level for a total of 27 low-lying states, subsequently used to extract binding energies, spectroscopic parameters, and bonding schemes. In addition, some 20 or more states for every MB species have been examined at the MRCI/4Z level of theory. The ground state symmetries and corresponding binding energies (in kcal/mol) are $^5\Sigma^-$(ScB), 76; $^6\Delta$(TiB), 65; $^7\Sigma^+$(VB), 55; $^6\Sigma^+$(CrB), 31; $^5\Pi$(MnB), 20; $^4\Sigma^-$(FeB), 54; $^3\Delta$(CoB), 66; $^2\Sigma^+$(NiB), 79; and $^1\Sigma^+$(CuB), 49. © *2008 American Institute of Physics*. [DOI: 10.1063/1.2821104]

I. INTRODUCTION

Boron is one of the most interesting elements of the periodic table. Next to carbon and diagonal to silicon, it shows an extraordinary bonding versatility rivaled only by that of carbon. Its electron "deficient" configuration, four valence orbitals and three electrons ($2s^2 2p^1$), gives rise to a remarkable binding agility with almost all elements and in any proportion. With transition metals, it forms solid borides, materials of high technological importance due to their unique physicochemical properties, namely, high melting points, involatility, high electrical conductivity, etc.[1]

The diatomic transition metal borides are the simplest building blocks of the very complex solid metal borides; therefore, an investigation of the electronic structure of the former can be proven useful in the field of the corresponding bulk materials, crystalline or otherwise.

Surprisingly, either experimental or theoretical work on the 3*d* MB neutral diatomics, M=Sc, Ti, V, Cr, Mn, Fe, Co, Ni, and Cu is very limited indeed. As far as we know, there is only one and rather obscure experimental work reporting a dissociation energy of 66.0 ± 15 kcal/mol for both ScB and TiB.[2] For the remaining seven MB borides, M=V to Cu, experimental results are completely absent from the literature. On the theoretical side, only two *ab initio* studies have been published so far. The first one by Barysz and Urban concerns the ground states ($^1\Sigma^+$) of the three boron-coinage metal diatomics CuB, AgB, and AuB.[3] For CuB, in particular, they performed CASPT2 and CCSD(T)/$[9s7p3d1f/_{Cu}$ $5s3p2d/_B]$ calculations, reporting bond distances, dissociation energies, harmonic and anharmonic frequencies, and electric dipole moments. The second study published in 2007 refers to triplet and quintet states of ScB through multireference CISD (MRCISD) and coupled-cluster [CCSD(T)] calculations.[4] For the two lowest states $X\ ^5\Sigma^-$ and $a\ ^3\Sigma^-$, the ANO-L (ANO stands for atomic natural orbital) $\equiv[7s6p5d4f3g/_{Sc}5s4p3d2f/_B]$ basis set was employed, whereas for the 14 higher states, seven triplets ($^3\Sigma^-$, $^3\Sigma^+$, $^3\Pi[3]$, $^3\Delta[2]$) and seven quintets ($^5\Sigma^+$, $^5\Pi[2]$, $^5\Delta[3]$, $^5\Phi$), the ANO-S$\equiv[5s4p3d2f/_{Sc}4s3p2d/_B]$ basis set was used. Potential energy curves are also reported at the MRCISD/ANO-S level of theory.[4]

Finally, it should be mentioned that multiconfigurational CI calculations on ScB^+, TiB^+, VB^+, and CrB^+ have been published by Kalemos and Mavridis.[5]

Presently, we report multireference variational calculations on the series MB, M=Sc to Cu. We examine, in particular, the first two (ScB), four (TiB), four (VB), three (CrB), three (MnB), two (FeB), two (CoB), two (NiB), and five (CuB) lowest states of the MB series. Following the pattern of our previous work on the diatomic metal carbides MC,[6] for all 27 states studied we report potential energy curves (PECs), total energies (E), bond distances (r_e), binding energies (D_e), dipole moments (μ), and common spectroscopic parameters (ω_e, $\omega_e x_e$, α_e, $\bar{D}_e$). We also try to resolve the bonding nature of these chemically simple but otherwise recondite species, through valence-bond-Lewis (vbL) diagrams and Mulliken distributions.

The purpose of this work is to color for the first time a picture of the MB (M=Sc to Cu) landscape, perhaps of practical importance for future experimental work on both condensed and gas phase 3*d* transition metal borides.

[a]Present address: Theoretical and Physical Chemistry Institute, National Hellenic Research Foundation, 48 Vassileos Constantinou Ave., Athens 116 35, Greece.
[b]Electronic mail: mavridis@chem.uoa.gr.

TABLE I. MRCI/5Z (MRCI+Q/5Z) [M_j-averaged experimental] (Ref. 13) atomic separation energies (in eV) of Sc, Ti, V, Cr, Mn, Fe, Co, Ni, Cu, and B atoms.

Sc		Ti		V	
$a\,^4F \leftarrow a\,^2D$	$a\,^2F \leftarrow a\,^2D$	$a\,^5F \leftarrow a\,^3F$	$a\,^1D \leftarrow a\,^3F$	$a\,^6D \leftarrow a\,^4F$	$a\,^4D \leftarrow a\,^4F$
1.573	1.859	0.877	1.005	0.238	1.007
(1.671)	(1.874)	(0.973)	(0.948)	(0.343)	(1.048)
[1.427]	[1.846]	[0.806]	[0.872]	[0.245]	[1.026]
Cr		Mn		Fe	
$a\,^5S \leftarrow a\,^7S$	$a\,^5D \leftarrow a\,^7S$	$a\,^6D \leftarrow a\,^6S$		$a\,^5F \leftarrow a\,^5D$	$a\,^3F \leftarrow a\,^5D$
0.924	1.200	1.963		0.933	1.548
(0.869)	(1.068)	(2.223)		(0.980)	(1.544)
[0.941]	[1.003]	[2.145]		[0.875]	[1.488]
Co		Ni		Cu	B
$b\,^4F \leftarrow a\,^4F$	$a\,^2F \leftarrow a\,^4F$	$a\,^3D \leftarrow a\,^3F$	$a\,^1D \leftarrow a\,^3F$	$a\,^2D \leftarrow a\,^2S$	$a\,^4P \leftarrow a\,^2P$
0.430	0.889	−0.047	0.251	1.676	3.598
(0.452)	(0.874)	(−0.051)	(0.218)	(1.664)	(3.627)
[0.417]	[0.879]	[−0.0298][a]	[0.302]	[1.490]	[3.571]

[a] $a\,^3D_{M_j=3} \leftarrow a\,^3F_{M_j=4}$=0.0254 eV.

II. COMPUTATIONAL APPROACH

To determine the relative order of the first 18–25 states for each molecule in the MB series, preliminary MRCI [= complete active space-self consistent field+single+double replacements (CASSCF+1+2)] calculations were performed using the Sc to Cu ANO basis sets of Bauschlicher, Jr.[7] $(21s16p9d6f4g)_{\mathrm{Sc-Ti}}$, $(20s15p10d6f4g)_{\mathrm{V-Cu}}$, and the Dunning, Jr.[8] correlation consistent basis set for B cc-pVQZ $=(12s6p3d2f1g)$, both generally contracted to $[7s6p4d3f2g/_{\mathrm{M}}5s4p3d2f1g/_{\mathrm{B}}](\equiv 4Z)$. This set contains 139 spherical Gaussians. Then, for the M atoms, the quintuple Z correlation consistent Balabanov and Peterson[9] bases were employed, i.e., cc-pV5Z$=(28s20p12d4f3g2h1i)_{\mathrm{M}}$ combined with the cc-pV5Z$=(14s8p4d3f2g1h)_{\mathrm{B}}$ basis set for B.[8] These sets were generally contracted to $[9s8p6d4f3g2h1i/_{\mathrm{M}}6s5p4d3f2g1h/_{\mathrm{B}}]$ $(\equiv 5Z)$ defining a 244 dimensional Gaussian orbital space.

The CASSCF reference wave functions are built by distributing 6 $[\mathrm{Sc}(3d^14s^2)+\mathrm{B}(2s^22p^1)]$ up to 14 $[\mathrm{Cu}(3d^{10}4s^1)+\mathrm{B}(2s^22p^1)]$ "valence" (active) electrons to ten orbital functions, one 4*s* and five 3*d*'s on M + one 2*s* and three 2*p*'s on B. Our reference spaces range from 112 (CrB; $a\,^8\Pi$) to 6884 (FeB; $A\,^2\Sigma^-$) configuration functions (CFs), with corresponding MRCI spaces ranging from about 9×10^6 (ScB; $X\,^5\Sigma^-$) to 10^9 (CuB; $b\,^3\Sigma^+$) CFs. These numbers are reduced by more than one or two orders of magnitude, respectively, through the internal contraction (icMRCI) scheme,[10] thus rendering the construction of PECs feasible.

All calculations were done under C_{2v} symmetry constraints; however, our CASSCF wave functions display correct axial angular momentum symmetry along the molecular axis, i.e., $|\Lambda|=0$, 1, 2, etc. It is useful to remember that the symmetry of the MRCI wave functions conforms to the symmetry species of the Abelian C_{2v} point group, i.e., A_1 (or A_2) and B_1 (or B_2).

Within the general spirit of the present work, which is to capture a general view of the trends and properties of the MB series, no further corrections due to semicore $3s^23p^6$ correlation effects of the metal atom were considered, or for that matter relativistic effects, except for ScB and TiB; our results are based on the "bare" icMRCI calculations. Our experience, however, with the 3*d* transition metal diatomics has shown us that uncorrected MRCI results can be quite quantitative due to cancellation of errors.[6]

The Davidson correction for unlinked quadruples (+Q) (Ref. 11) was used to ameliorate significant size nonextensivity problems, particularly for the late transition metal borides. All calculations were performed with the MOLPRO 2002 suite of codes.[12]

III. RESULTS AND DISCUSSION

Atomic separation energies for the first or the first two excited states of the ten atoms involved in the present calculations along with experimental results,[13] are given in Table I. As can be seen, the theoretical values are in reasonable agreement with the experimental ones.

Total energies (E), equilibrium bond distances (r_e), dissociation energies (D_e) with respect to the adiabatic products, harmonic frequencies and anharmonic corrections ($\omega_e, \omega_e x_e$), rotational vibrational couplings (α_e), centrifugal distortions ($\bar{D}_e$), gross Mulliken charges (q_M), dipole moments (μ), and energy separations (T_e) at the CASSCF and icMRCI(+Q)/$[9s8p6d4f3g2h1i/_{\mathrm{M}}6s5p4d3f2g1h/_{\mathrm{B}}]$ $(\equiv 5Z)$ level of theory for the nine MB molecules are listed in Table II.

The MRCI/5Z PECs of the first two or up to five lowest states of each metal boride are shown in Figs. 1 (ScB) to 9 (CuB). In addition, an inset in every figure depicts a relative energy level diagram of about 20 states calculated at the MRCI+Q/4Z level of theory.

TABLE II. Absolute energies E (hartree), bond lengths r_e (Å), binding energies D_e (kcal/mol), harmonic frequencies and anharmonic corrections ω_e, $\omega_e x_e$ (cm^{-1}), rotational vibrational couplings α_e (cm^{-1}), centrifugal distortions $\bar{D}_e$ (cm^{-1}), total Mulliken charges on the metal q_M, dipole moments μ (Debye), and energy differences T_e (kcal/mol) of the metal borides ($M^{11}B$), M=Sc to Cu.

Molecule	State	Method[a]	$-E$	r_e	D_e	ω_e	$\omega_e x_e$	$\alpha_e(10^{-3})$	$\bar{D}_e(10^{-6})$	q_M	$\langle\mu\rangle$[b]	μ_{FF}[b]	T_e
ScB	$X\,^6\Sigma^-$	CASSCF	784.36868	2.121	67.7	597.3	3.86	3.11	0.85	0.20	3.65	3.65	0.0
		MRCI	784.43926	2.128	75.1	584.5	3.80	3.28	0.87	0.18	4.02	4.16	0.0
		MRCI+Q	784.4434	2.132	75.8	579	3.8	3.3	0.88			4.23	0.0
		C-MRCI+DKH2[c]	788.31006	2.092	73.7	608.2	2.76	3.21	0.89	0.46	3.68	3.99	0.0
		C-MRCI+DKH2+Q[c]	788.3449	2.094	76.3	603	2.6	3.3	0.91			4.13	0.0
		Expt.[d]			66.0 ± 15								
	$a\,^3\Sigma^-$	CASSCF	784.36429	2.231	37.2	468.3	3.14	3.63	1.03	0.19	2.36	2.36	2.8
		MRCI	784.43649	2.238	37.9	468.7	2.50	3.52	1.00	0.20	2.74	2.89	1.7
		MRCI+Q	784.4416	2.249	36.9	467	2.8	3.0	0.98			2.89	1.1
		C-MRCI+DKH2[c]	788.30436	2.195	36.7	490.7	2.31	4.27	1.03	0.44	2.38	2.73	3.6
		C-MRCI+DKH2+Q[c]	788.3397	2.200	38.9	487	2.1	4.2	1.0			2.84	3.2
TiB	$X\,^6\Delta$	CASSCF	873.02641	2.086	49.1	583.8	3.63	3.45	0.95	0.12	2.78	2.78	0.0
		MRCI	873.12852	2.077	62.8	587.6	3.50	3.45	0.96	0.11	3.13	3.42	0.0
		MRCI+Q	873.1358	2.080	64.5	583	3.5	3.5	1.0			3.51	0.0
		Expt.[d]			66.0 ± 15								
	$1\,^4\Delta$	CASSCF	873.01291	2.245	23.7	388.3	3.98			0.17	1.34	1.34	8.5
		MRCI	873.11497	2.188	34.5	436.1	4.70	7.18	1.26	0.15	1.74	2.00	8.5
		MRCI+Q	873.1232	2.214	34.6	427						2.10	7.9
	$2\,^4\Pi_G$	CASSCF	873.01378	1.948	25.5	588.5	6.23	4.96	1.26	0.07	2.59	2.59	7.9
		MRCI	873.11481	1.962	34.5	618.9	4.58	4.40	1.22	0.05	2.89	3.36	8.6
		MRCI+Q	873.1235	1.964	34.7	618	4.6	4.4	1.2			3.37	7.7
	$2\,^4\Pi_L$	CASSCF	873.00284	2.460	18.7	383.0	2.89	2.85	0.82	0.28	2.56	2.57	14.8
		MRCI	873.09852	2.364	24.2	400.4	3.8			0.22	2.37	2.55	18.8
		MRCI+Q	873.1075	2.347	24.7	410	4.1					2.45	17.8
	$3\,^2\Sigma^+$	CASSCF	873.02166	1.899	59.4	649.4	4.59	4.48	1.35	0.02	1.03	1.03	3.0
		MRCI	873.11366	1.913	35.7	657.5	3.80	3.94	1.26	0.01	1.79	2.13	9.3
		MRCI+Q	873.1202	1.924	34.6	642	3.5	4.0	1.3			2.29	9.8
VB	$X\,^7\Sigma^+$	CASSCF	967.50106	2.050	36.8	590.4	3.33	3.39	1.00	0.09	2.52	2.52	0.0
		MRCI	967.63544	2.039	52.3	589.9	3.75	3.66	1.03	0.06	2.73	3.20	0.0
		MRCI+Q	967.6460	2.043	54.9	585	3.8	3.7	1.0			3.30	0.0
	$a\,^5\Pi$	CASSCF	967.48932	1.960	26.2	592.6	4.81	4.70	1.30	0.07	2.29	2.29	7.4
		MRCI	967.62690	1.938	40.6	615.6	4.39	4.51	1.29	0.03	2.48	2.91	5.4
		MRCI+Q	967.6376	1.942	42.0	610	4.5	4.6	1.3			3.01	5.3
	$b\,^5\Phi$	CASSCF	967.49036	1.960	26.9	597.6	4.70	4.56	1.27	0.08	2.27	2.27	6.7
		MRCI	967.62600	1.940	40.0	616.3	4.33	4.47	1.28	0.04	2.43	2.81	5.9
		MRCI+Q	967.6364	1.944	41.1	610	4.4	4.6	1.3			2.90	6.0
	$c\,^5\Delta$	CASSCF	967.48277	2.181	22.1	444.5	3.55	1.60	1.21	0.19	2.56	2.56	11.5
		MRCI	967.62178	2.159	37.2	476.7	4.47	2.14	1.12	0.13	2.34	2.39	8.6
		MRCI+Q	967.6341	2.170	39.7	477	5.0	2.5	1.1			2.19	7.5
CrB	$X\,^6\Sigma^+$	CASSCF	1067.93239	2.553	7.64	215.6	3.66	4.37	1.99	0.11	1.51	1.51	0.0
		MRCI	1068.10188	2.166	26.3	420.0	18.5	7.85	1.41	0.08	1.43	2.05	0.0
		MRCI+Q	1068.1177	2.183	31.2	405	20	7.6	1.5			1.99	0.0
	$A\,^6\Pi$	CASSCF	1067.92564	2.000	4.68	479.5	21.4	10.4	1.75_+	0.11	2.44	2.44	4.24
		MRCI	1068.10010	1.995	25.3	459.6	0.77	8.89	1.92	0.08	2.54	3.12	1.12
		MRCI+Q	1068.1144	2.001	29.1	462						3.23	2.1
	$a\,^8\Pi$	CASSCF	1067.92255	2.379	2.73	253.9	9.78	8.99	2.19	0.28	3.89	3.89	6.18
		MRCI	1068.09246	2.182	20.5	417.5	4.07	6.60	1.36	0.24	3.73	3.83	5.91
		MRCI+Q	1068.1071	2.161	24.5	441	4.7	6.7	1.3			3.65	6.6
MnB	$X\,^5\Pi$	CASSCF	1174.44318	2.316	9.48	382.9	4.22	3.67	1.10	0.38	2.73	2.73	0.0
		MRCI	1174.63356	2.190	19.5	391.9	3.79	3.37	1.47	0.28	2.21	2.45	0.0
		MRCI+Q	1174.6495	2.183	19.7	383	3.9	3.6	1.6			2.39	0.0
	$A\,^5\Sigma^-$	CASSCF	1174.42309	1.951	72.4	448.9	1.73	6.18	2.24	0.26	2.41	2.41	12.6
		MRCI	1174.62920	1.832	71.4	635.8	4.38	5.18	1.62	0.05	1.93	2.44	2.74
		MRCI+Q	1174.6462	1.832	72.2	643	4.1	4.9	1.6			2.50	2.1
	$a\,^7\Pi$	CASSCF	1174.43564	2.382	4.76	370.1	6.01	4.58	0.99	0.40	2.72	2.72	4.73
		MRCI	1174.62144	2.343	11.9	351.1	6.01	5.21	1.22	0.34	2.40	2.57	7.61

TABLE II. (*Continued.*)

Molecule	State	Method[a]	$-E$	r_e	D_e	ω_e	$\omega_e x_e$	$\alpha_e(10^{-3})$	$\bar{D}_e(10^{-6})$	q_M	$\langle\mu\rangle$[b]	μ_{FF}[b]	T_e
		MRCI+Q	1174.6374	2.357	12.2	330	6.4	5.8	1.3			2.45	7.6
FeB	$X\,^4\Sigma^-$	CASSCF	1287.05963	1.772	32.7	547	22.0	16.5	2.65	0.01	2.00	2.00	0.0
		MRCI	1287.32935	1.743	53.1	642.7	12.5	10.0	2.12	−0.07	1.67	2.13	0.0
		MRCI+Q	1287.3522	1.747	54.1	645	13.2	9.9	2.1			2.20	0.0
	$a\,^2\Sigma^-$	CASSCF	1287.04859	1.752	81.5	704.5	3.47	4.20	1.72	−0.05	2.08	2.08	6.9
		MRCI	1287.31979	1.725	82.4	768.9	3.90	4.26	1.58	−0.12	1.72	2.21	6.0
		MRCI+Q	1287.3431	1.726	83.8	773	4.1	4.4	1.6			2.24	5.7
CoB	$X\,^3\Delta$	CASSCF	1406.03586	1.711	36.6	708.0	7.95	7.17	1.91	−0.07	1.34	1.34	0.0
		MRCI	1406.37624	1.696	63.1	756.9	6.14	5.92	1.76	−0.14	1.03	1.83	0.0
		MRCI+Q	1406.4059	1.700	65.7	757	6.1	5.9	1.7			1.98	0.0
	$a\,^1\Delta$	CASSCF	1406.02838	1.713	79.2	736.2	3.11	4.45	1.75	−0.09	1.62	1.62	4.70
		MRCI	1406.37100	1.700	80.7	788.8	3.57	3.96	1.60	−0.16	1.28	2.25	3.29
		MRCI+Q	1406.4013	1.704	83.2	791	3.7	4.0	1.6			2.38	2.86
NiB	$X\,^2\Sigma^+$	CASSCF	1531.49875	1.682	41.2	779.7	4.38	5.10	1.76	−0.11	1.12	1.12	0.0
		MRCI	1531.91879	1.676	74.7	805.1	3.93	4.56	1.68	−0.17	0.80	2.16	0.0
		MRCI+Q	1531.9563	1.681	79.2	803.0	3.98	4.53	1.66			2.41	0.0
	$A\,^2\Delta$	CASSCF	1531.48605	1.903	33.3	491.4	8.10	12.5	2.08	0.01	2.80	2.80	7.97
		MRCI	1531.88848	1.892	55.4	599.8	3.12	3.83	1.47	−0.03	1.41	1.85	19.0
		MRCI+Q	1531.9278	1.890	61.2	603.5	3.31	3.87	1.46			1.58	17.9
CuB	$X\,^1\Sigma^+$	MRCI	1664.08293	1.934	42.4	496.9	5.54	6.63	1.80	−0.01	1.21	1.71	0.0
		MRCI+Q	1664.1282	1.922	49.1	553	4.8	4.6	1.5			1.62	0.0
	$a\,^3\Pi$	MRCI	1664.05736	1.904	25.8	560.8	10.0	3.22	1.55	0.17	3.47	3.31	16.0
		MRCI+Q	1664.1021	1.885	31.5	569	4.4	4.4	1.6			3.08	16.4
	$A\,^1\Sigma^+$	MRCI	1664.05668	1.830	63.3	702.0	5.29	4.02	1.26	−0.04	0.30	1.34	16.5
		MRCI+Q	1664.1054	1.828	71.7	714.5	6.19	4.0	1.2			1.30	14.3
	$B\,^1\Pi$	MRCI	1664.02628	1.995	6.2	333				0.21	2.45	2.92	35.5
		MRCI+Q	1664.0708	1.936	11.9	426						2.81	36.0
	$b\,^3\Sigma^+$	MRCI	1664.02157	1.912	2.9	510	10.6	10.7	1.83	−0.12	2.63	2.86	38.5
		MRCI+Q	1664.0631	1.933	6.9	463						2.94	40.9

[a]Internally contracted MRCI; +Q refers to the multireference Davidson correction.
[b]$\langle\mu\rangle$ refers to expectation values and μ_{FF} to finite field values (field strength 10^{-4} a.u.).
[c]C-MRCI+DKH2(+Q)/cc-pwCV5Z.
[d]Reference 2.

In what follows, Secs. III A–III I, we analyze each MB molecule separately.

A. ScB

The two lowest states of ScB, well separated from the rest, are of symmetries $^5\Sigma^-$ and $^3\Sigma^-$ with the former being almost certainly the ground state (*vide infra*). The $^5\Sigma^-$ state correlates to $\mathrm{Sc}(a\,^4F)+\mathrm{B}(^2P)$, whereas the $^3\Sigma^-$ to the ground state atoms $\mathrm{Sc}(a\,^2D)+\mathrm{B}(^2P)$. The leading equilibrium CASSCF configurations, followed by the Mulliken atomic distributions (Sc/B), are

$$|X\,^5\Sigma^-\rangle_{A_2} \approx 0.94|1\sigma^2 2\sigma^1 3\sigma^1 1\pi_x^1 1\pi_y^1\rangle,$$

$$4s^{1.00}4p_z^{0.29}3d_{z^2}^{0.64}3d_{xz}^{0.37}4p_x^{0.06}3d_{yz}^{0.37}4p_y^{0.06}3d_{x^2-y^2}^{0.00}3d_{xy}^{0.00}/$$
$$2s^{1.47}2p_z^{0.55}2p_x^{0.56}2p_y^{0.56}$$

and

$$|\alpha\,^3\Sigma^-\rangle_{A_2} \approx |[0.81(1\sigma^2 2\sigma^2) - 0.38(1\sigma^2 3\sigma^2)]1\pi_x^1 1\pi_y^1\rangle$$
$$- 0.25|1\sigma^2 2\sigma^1 3\sigma^1 1\bar{\pi}_x^1 1\pi_y^1\rangle,$$

$$4s^{1.08}4p_z^{0.44}3d_{z^2}^{0.21}3d_{xz}^{0.48}4p_x^{0.05}3d_{yz}^{0.48}4p_y^{0.05}3d_{x^2-y^2}^{0.00}3d_{xy}^{0.00}/$$
$$2s^{1.52}2p_z^{0.70}2p_x^{0.46}2p_y^{0.46}.$$

Notice that only the six valence electrons are counted, whereas, the 20 "core" electrons $(1s^2 2s^2 2p^6 3s^2 3p^6/_{\mathrm{Sc}} 1s^2/_{\mathrm{B}})$ have been suppressed. The bonding in both states can be captured by the following vbL diagrams, based on the leading CFs and the atomic Mulliken distributions.

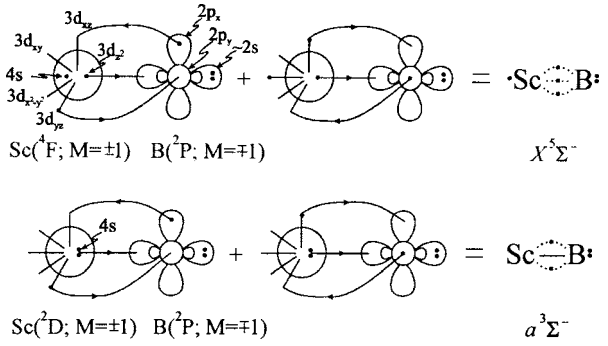

The bonding in the $X\,^5\Sigma^-$ state comprises two half π and one

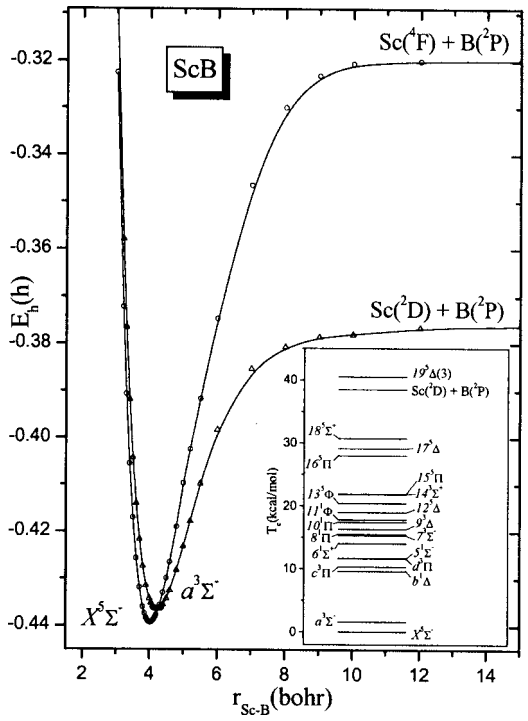

FIG. 1. MRCI/5Z potential energy curves of the ScB molecule. All energies shifted by $+784.0E_h$. Inset: MRCI+Q/4Z relative energy levels of 20 states of the ScB molecule.

half σ bonds $(\frac{1}{2}\sigma,\frac{1}{2}\pi,\frac{1}{2}\pi)$ and two half π and one σ bond $(\sigma,\frac{1}{2}\pi,\frac{1}{2}\pi)$ in the $a\ ^3\Sigma^-$ state. In both states, a total of about $0.2e^-$ are transferred from the metal to the B atom according to the total Mulliken populations.

From Table II, we can see that the MRCI(+Q)/5Z binding energies of the $X\ ^5\Sigma^-$ and $a\ ^3\Sigma^-$ states with respect to the adiabatic channels are D_e=75.1 (75.8) and 37.9 (36.9) kcal/mol at r_e=2.128 (2.132) and 2.238 (2.249) Å, respectively. Correcting for the zero point energy (ZPE $\approx\omega_e/2$), we get D_0=74.3 (75.0) and 37.3 (36.3) kcal/mol. Note that the $X\ ^5\Sigma^-$ state has much higher binding energy as compared to $a\ ^3\Sigma^-$ since it opens adiabatically to an excited Sc $(a\ ^4F;s^1d^2)$ atom, while the $a\ ^4\Sigma^-$ state opens to the ground state of the Sc atom $(a\ ^2D;s^2d^1)$. The atomic separation energy of Sc $a\ ^4F\leftarrow a\ ^2D$ at the MRCI/5Z(experimental) level is 1.573 (1.427) eV (see Table I).

The $a\ ^3\Sigma^-$ state is above the $X\ ^5\Sigma^-$ by 1.7 (1.1) kcal/mol $(=T_e)$, or $T_0=T_e+\Delta\omega_e/2$=1.5 (0.95) kcal/mol. Using the weighted core correlation consistent basis set of quintuple cardinality of Balabanov and Peterson, cc-pwCV5Z contracted to [11*s*10*p*8*d*5*f*4*g*3*h*2*i*],[9] core ($3s^23p^6$ of Sc) correlation effects were taken into account, as well as scalar relativistic effects through the second order Douglas-Kroll-Hess approximation.[14] At this level of theory, C-MRCI+DKH2 (+Q)/cc-pwCV5Z, the ordering between the $^5\Sigma^-$-$^3\Sigma^-$ energy separation now becomes T_e=3.6 (3.2) kcal/mol. Therefore, we can claim with some confidence that the ground state of ScB molecule is of $^5\Sigma^-$ symmetry. Moreover, at the C-MRCI+DKH2(+Q)/cc-pwCV5Z level for the $X\ ^5\Sigma^-$ state, we calculate r_e=2.092 (2.094) Å, D_e=73.7 (76.3) kcal/mol, and $\langle\mu\rangle/\mu_{\mathrm{FF}}$=3.68/3.99 D, where $\langle\mu\rangle$ and μ_{FF} are expectation value and finite field dipole moments, respectively. Notice that while the binding energy remains practically the same from MRCI+Q/5Z to C-MRCI+DKH2 +Q/cc-pwCV5Z, 75.8 versus 76.3 kcal/mol, the bond distance and dipole moment decrease by 0.04 Å and 0.1 Debye (μ_{FF}), respectively. For the $a\ ^3\Sigma^-$ state, completely analogous results are obtained at the C-MRCI +DKH2/cc-pwCV5Z level of theory; i.e., the r_e and μ_{FF} values decrease by about 0.04 Å and 0.16 D, whereas D_e remains practically the same, as contrasted to the plain MRCI/5Z values. The above discussion shows that our uncorrected results with respect to core-valence correlation and scalar relativistic effect MRCI results can be considered as quite reliable.

The C-MRCI/$[7s6p5d4f3g/_{\mathrm{Sc}}\ 5s4p3d2f/_{\mathrm{B}}]$ results of Černušák *et al.*[4] are similar to the present ones for both $X\ ^5\Sigma^-$ (r_e=2.120 Å, D_e=75.8 kcal/mol) and $a\ ^3\Sigma^-$ states (r_e=2.211 Å, D_e=39.2 kcal/mol); however, a difference of 0.6 D is observed in the $\langle\mu\rangle$ dipole moment value of the $X\ ^5\Sigma^-$ state.

The PECs of the two lowest states are plotted in Fig. 1; the inset shows the relative energy ordering of 20 states of ScB. The second excited state, $b\ ^1\Delta$, lies about 9 kcal/mol above the ground state at the MRCI+Q/5Z level of theory.

Finally, comparing the neutral ScB molecule with the ScB^+ cation,[5(a)] we observe that the $X\ ^4\Sigma^-$ state of ScB^+ results from the $X\ ^5\Sigma^-$ of ScB by removing an electron from the σ frame of ScB. The r_e values of ScB and ScB^+ are similar, but the D_e of ScB^+ is 45 kcal/mol at the MRCI/$[7s6p4d3f/_{\mathrm{Sc}}\ 4s3p2d1f/_{\mathrm{B}}]$ level, about 30 kcal/mol less than that of the ScB molecule.

B. TiB

Figure 2 shows four PECs of the TiB molecule and a relative energy diagram (inset) of the first 20 states. The ground state, $X\ ^6\Delta$, is well separated (≈9 kcal/mol) from the first three excited states ($1\ ^1\Delta, 2\ ^4\Pi, 3\ ^2\Sigma^+$), which are practically degenerate. The $X\ ^6\Delta$ state correlates to the first excited state of the metal, Ti$(4s^13d^3;a\ ^5F)$, experimentally 18.6 kcal/mol above its ground state $^3F(4s^23d^2)$.[13]

The MRCI(+Q)/5Z D_e and r_e values are 62.8 (64.5) kcal/mol and 2.077 (2.080) Å, respectively. Extending our calculations to the C-MRCI+DKH2 +Q/cc-pwCV5Z level of theory, the D_e of $X\ ^6\Delta$ remains practically the same whereas, r_e decreases by 0.03 Å, a similar behavior as in the $X\ ^5\Sigma^-$ and $a\ ^3\Sigma^-$ states of ScB. An experimental D_e estimate of 66.0 ± 15 kcal/mol (the same value is also given for ScB) is cited in the literature,[2] but obviously cannot be considered as very reliable.

The leading equilibrium CASSCF CFs and the ensuing atomic Mulliken populations are

$$|X\ ^6\Delta\rangle_{A_1+A_2}\approx 0.93/\sqrt{2}|1\sigma^2 2\sigma^1 3\sigma^1 1\pi_x^1 1\pi_y^1(1\delta_-^1+1\delta_+^1)\rangle,$$

$$4s^{0.99}4p_z^{0.25}3d_{z^2}^{0.68}3d_{xz}^{0.43}4p_x^{0.05}3d_{yz}^{0.43}4p_y^{0.05}3d_{x^2-y^2}^{0.50}3d_{xy}^{0.50}/$$

$$2s^{1.50}2p_z^{0.54}2p_x^{0.52}2p_y^{0.52}.$$

The following vbL diagrams show that the bonding scheme

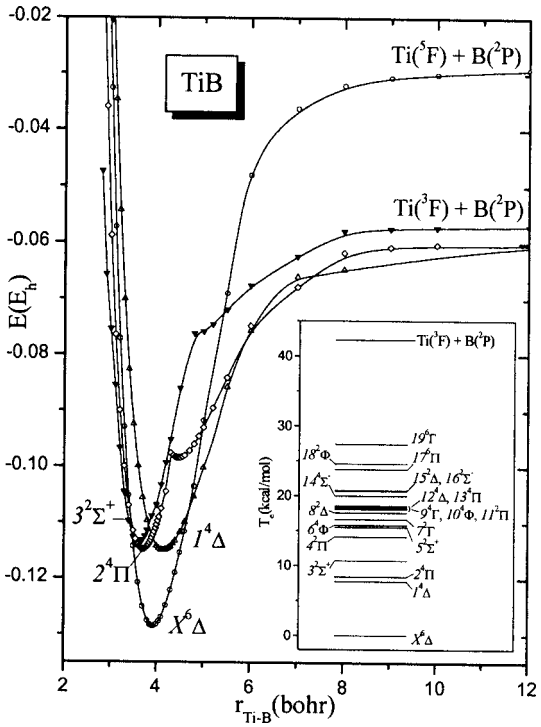

FIG. 2. MRCI/5Z potential energy curves of the TiB molecule. All energies shifted by $+873.0E_h$. Inset: MRCI+Q/4Z relative energy levels of 20 states of the TiB molecule.

consists of three half bonds $(\frac{1}{2}\sigma,\frac{1}{2}\pi,\frac{1}{2}\pi)$, exactly as in the $X\,^5\Sigma^-$ state of ScB.

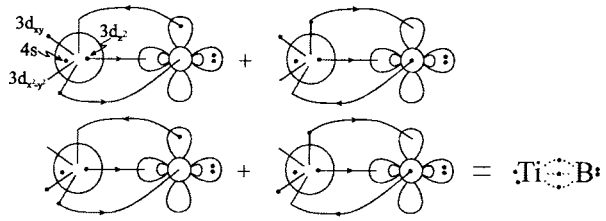

The next two states, $1\,^4\Delta$ and $2\,^4\Pi$, are degenerate at the MRCI(+Q)/5Z level, the labeling "1" and "2" being only formal, lying 8.5 (7.9) and 8.6 (7.7) above the $X\,^6\Delta$ state, whereas the $3\,^2\Sigma^+$ is 9.3 (9.8) kcal/mol higher. They all correlate adiabatically to the ground state atoms, $\mathrm{Ti}(^3F)+\mathrm{B}(^2P)$. At around 7 bohrs, the $1\,^4\Delta$ state interacts with the $12\,^4\Delta$ state (see inset of Fig. 2), which also correlates to $\mathrm{Ti}(a\,^3F)+\mathrm{B}(^2P)$; the $2\,^4\Pi$ suffers an avoided crossing at 4.3 bohrs with $14\,^4\Pi$, which correlates to $\mathrm{Ti}(a\,^5F)+\mathrm{B}(^2P)$; $3\,^2\Sigma^+$ displays an avoided crossing at 4.7 bohrs with the $5\,^2\Sigma^+$ state, the latter correlating to the ground state fragments. The main equilibrium CASSCF CFs, atomic population densities, and vbL diagrams are given below,

$$|1\,^4\Delta\rangle_{A_1} \approx |[0.80(1\sigma^2 2\sigma^2) - 0.39(1\sigma^2 3\sigma^2)]1\pi_x^1 1\pi_y^1 1\delta_-^1\rangle - 0.24|1\sigma^2 2\sigma^2 2\pi_x^1 2\pi_y^1 1\delta_-^1\rangle,$$

$$4s^{1.04}4p_z^{0.40}3d_{z^2}^{0.17}3d_{xz}^{0.59}4p_x^{0.03}3d_{yz}^{0.59}4p_y^{0.03}3d_{x^2-y^2}^{0.50}3d_{xy}^{0.50}/2s^{1.59}2p_z^{0.76}2p_x^{0.39}2p_y^{0.39},$$

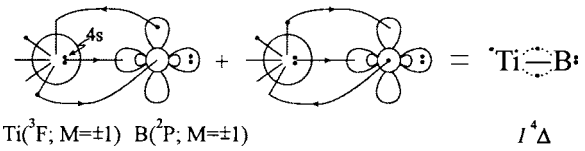

$$|2\,^4\Pi\rangle_{B_1} \approx |1\sigma^2 2\sigma^1 3\sigma^1 1\pi_x^1[0.84(1\pi_y^2) - 0.18(2\pi_y^2)]\rangle - 0.18|1\sigma^2 2\sigma^1(1\pi_x^2 1\pi_y^1 1\delta_-^1 + 1\pi_x^1 1\pi_y^2 1\delta_+^1)\rangle,$$

$$4s^{0.99}4p_z^{0.32}3d_{z^2}^{0.69}3d_{xz}^{0.86}4p_x^{0.04}3d_{yz}^{0.86}4p_y^{0.04}3d_{x^2-y^2}^{0.07}3d_{xy}^{0.07}/2s^{1.41}2p_z^{0.49}2p_x^{0.58}2p_y^{0.58},$$

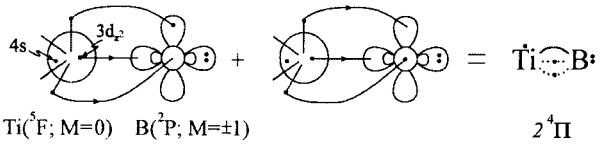

$$|3\,^2\Sigma^+\rangle_{A_1} \approx |1\sigma^2 2\sigma^1[0.89(1\pi_x^2 1\pi_y^2) - 0.21(2\pi_x^2 1\pi_y^2 + 1\pi_x^2 2\pi_y^2)]\rangle,$$

$$4s^{0.95}4p_z^{0.44}3d_{z^2}^{0.18}3d_{xz}^{1.17}4p_x^{0.04}3d_{yz}^{1.17}4p_y^{0.04}3d_{x^2-y^2}^{0.0}3d_{xy}^{0.0}/2s^{1.29}2p_z^{0.13}2p_x^{0.77}2p_y^{0.77}.$$

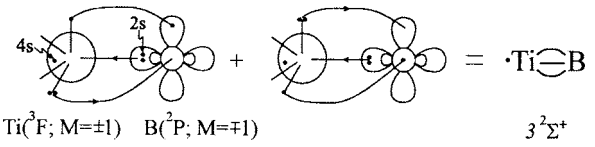

The MRCI+Q/5Z D_e values of the three states with respect to the ground state products are the same, D_e =34.6 kcal/mol. However, diabatically, the binding energy of the $2\,^4\Pi$ state is 56.7 kcal/mol. The $1\,^4\Delta$ features one σ and two half π bonds $(\sigma,\frac{1}{2}\pi,\frac{1}{2}\pi)$; $2\,^4\Pi$ one π, a half σ, and a half π $(\frac{1}{2}\sigma,\frac{1}{2}\pi,\pi)$, and the $3\,^2\Sigma^+$ state three genuine bonds, one σ and two π (σ,π,π). Consistently, the latter has the smaller bond distance [r_e=1.913 (1.924) Å] and the larger harmonic frequency [ω_e=657.5 (642) cm^{-1}], as compared to the $X\,^6\Delta$, $1\,^4\Delta$, and $2\,^4\Pi$ states.

The PECs of the four lowest states are depicted in Fig. 2; the inset shows the MRCI+Q relative energy ordering of 20 low-lying states of TiB. Some of them are degenerate, for example, $9\,^4\Gamma$, $10\,^4\Phi$, $11\,^2\Pi$, $12\,^4\Delta$, and $13\,^4\Pi$, so the numbering is purely formal.

Comparing the ground state of the neutral TiB molecule, $X\,^6\Delta$, with the ground state of TiB^+ cation, $X\,^5\Delta$,[5(b)] we observe that both have the Ti atom or Ti^+ excited with three half bonds $(\frac{1}{2}\sigma,\frac{1}{2}\pi,\frac{1}{2}\pi)$, but the *in situ* atoms have different M values, so the $X\,^5\Delta(\mathrm{TiB}^+)$ results from the $X\,^6\Delta(\mathrm{TiB})$ by abstracting one e^- followed by a "rearrangement" of M values. The $X\,^5\Delta(\mathrm{TiB}^+)$ PEC presents a minimum at 2.104 Å with D_e=49.0 kcal/mol at the MRCI+Q/$[7s6p4d3f/_{\mathrm{Cr}}\,4s3p2d1f/_{\mathrm{B}}]$[5(b)] level.

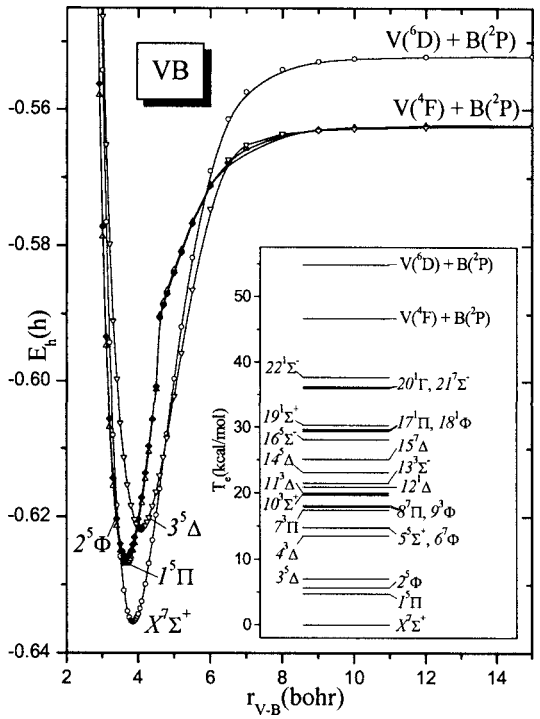

FIG. 3. MRCI/5Z potential energy curves of the VB molecule. All energies shifted by $+967.0E_h$. Inset: MRCI+Q/4Z relative energy levels of 23 states of the VB molecule.

C. VB

Figure 3 depicts MRCI/5Z PECs of the first four lowest states, namely, $X\,^7\Sigma^+$, $1\,^5\Pi$, $2\,^5\Phi$, and $3\,^5\Delta$; a relative energy diagram of 23 states calculated at the MRCI+Q/4Z level is shown in the inset.

Remarkably, the ground state is of $^7\Sigma^+$ symmetry, the highest multiplicity of all the nine MB ground states studied. It correlates adiabatically to the first excited state of $V(a\,^6D;sd^4)$, experimentally 0.245 eV above the $V(a\,^4F;sd^4)$,[13] maintaining this character to the equilibrium. The labeling of the next two states $1\,^5\Pi$ and $2\,^5\Phi$, "1" and "2," is only formal, being degenerate within less than 1 kcal/mol (Table II). The three quintets $1\,^5\Pi$, $2\,^5\Phi$, and $3\,^5\Delta$ correlate adiabatically to the ground state atoms $V(a\,^4F)+B(^2P)$, but diabatically to $V(a\,^6D)+B(^2P)$ due to avoided crossings at about 4.7, 4.7, and 6 bohrs, respectively.

The leading equilibrium CASSCF CFs, their atomic Mulliken population, and bonding as pictured by the vbL diagram of the four states above follow

$$|X\,^7\Sigma^+\rangle_{A_1} \approx 0.93|1\sigma^2 2\sigma^1 3\sigma^1 1\pi_x^1 1\pi_y^1 1\delta_+^1 1\delta_-^1\rangle,$$

$$4s^{0.95}4p_z^{0.18}3d_{z^2}^{0.76}3d_{xz}^{0.47}4p_x^{0.04}3d_{yz}^{0.47}4p_y^{0.04}3d_{x^2-y^2}^{0.99}3d_{xy}^{0.99}/$$
$$2s^{1.54}2p_z^{0.52}2p_x^{0.49}2p_y^{0.49},$$

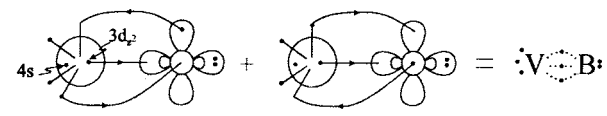

$$|1\,^5\Pi\rangle_{B_1(+)} \text{ or } |2\,^5\Phi\rangle_{B_1(-)} \approx 0.62|1\sigma^2 2\sigma^1 3\sigma^1(1\pi_x^2 1\pi_y^1 1\delta_-^1 \pm 1\pi_x^1 1\pi_y^2 1\delta_+^1)\rangle,$$

$$4s^{0.99}4p_z^{0.28}3d_{z^2}^{0.79}3d_{xz}^{0.91}4p_x^{0.03}3d_{yz}^{0.91}4p_y^{0.03}3d_{x^2-y^2}^{0.50}3d_{xy}^{0.50}/$$
$$2s^{1.45}2p_z^{0.46}2p_x^{0.56}2p_y^{0.56},$$

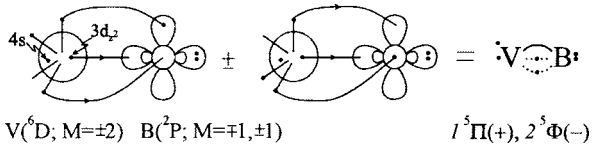

$$|3\,^5\Delta\rangle_{A_1+A_2} \approx \frac{1}{\sqrt{2}}|[0.83(1\sigma^2 2\sigma^2 3\sigma^1) - 0.21(1\sigma^2 3\sigma^1 4\sigma^2)] \times (1\pi_x^1 1\pi_y^1 1\delta_-^1 + 1\pi_x^1 1\pi_y^1 1\delta_+^1)\rangle,$$

$$4s^{1.07}4p_z^{0.29}3d_{z^2}^{0.96}3d_{xz}^{0.70}4p_x^{0.02}3d_{yz}^{0.70}4p_y^{0.02}3d_{x^2-y^2}^{0.52}3d_{xy}^{0.52}/$$
$$2s^{1.68}2p_z^{0.89}2p_x^{0.29}2p_y^{0.29}.$$

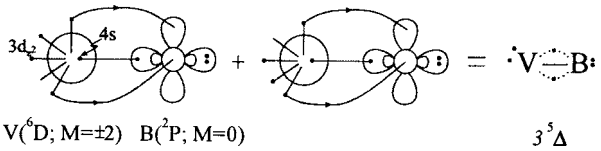

The bonding in the $X\,^7\Sigma^+$ state consists of three half bonds $(\frac{1}{2}\sigma,\frac{1}{2}\pi,\frac{1}{2}\pi)$, in $1\,^5\Pi$ and $2\,^5\Phi$ of $(\frac{1}{2}\sigma,\frac{1}{2}\pi,\pi)$ and in $3\,^5\Delta$ of $(\sigma,\frac{1}{2}\pi,\frac{1}{2}\pi)$. The MRCI(+Q)/5Z D_e (kcal/mol) and r_e (Å) values are 52.3 (54.9) and 2.039 (2.043), 40.6 (42.0) and 1.938 (1.942), 40.0 (41.1) and 1.940 (1.944), and 37.2 (39.7) and 2.159 (2.172) for the $X\,^7\Sigma^+$, $1\,^5\Pi$, $2\,^5\Phi$, and $3\,^5\Delta$ states, respectively (Table II).

Comparing the neutral VB molecule with the VB^+ cation,[5(c)] we observe that the $X\,^6\Sigma^+$ state of VB^+ presents an avoided crossing; in the equilibrium, the *in situ* V^+ cation is in its first excited state $a\,^5F$, whereas the bonding comprises three half bonds $(\frac{1}{2}\sigma,\frac{1}{2}\pi,\frac{1}{2}\pi)$ similar to $X\,^7\Sigma^+$ of VB. The r_e values of the two species are alike, but the D_e value of VB^+ is 45.5 kcal/mol at the MRCI +Q/$[7s6p4d3f/_{\mathrm{Cr}}\ 4s3p2d1f/_{\mathrm{B}}]$, about 10 kcal/mol less than the corresponding value of the $VB(X\,^7\Sigma^+)$ molecule.

D. CrB

The MRCI/5Z PECs for the $X\,^6\Sigma^+$, $A\,^6\Pi$, and $a\,^8\Pi$ states of CrB, along with the relative energies (MRCI+Q/4Z) of 20 states (inset), are shown in Fig. 4. The three lowest states correlate to the ground state fragments $Cr(a\,^7S;4s^13d^5)+B(^2P)$. However, close to equilibrium, the $X\,^6\Sigma^+$ state interacts strongly with the 25 kcal/mol higher $8\,^6\Sigma^+$ state, which correlates to $Cr(a\,^5S;4s^13d^5)+B(^2P)$; this can also be seen from the morphology of the $X\,^6\Sigma^+$ PEC at 4.2 bohrs. The equilibrium bond distance and the dissociation energies of the $X\,^6\Sigma^+$ state are r_e=2.166 (2.183) Å, D_e=26.3 (31.2) kcal/mol, with corresponding values for the $A\,^6\Pi$ and

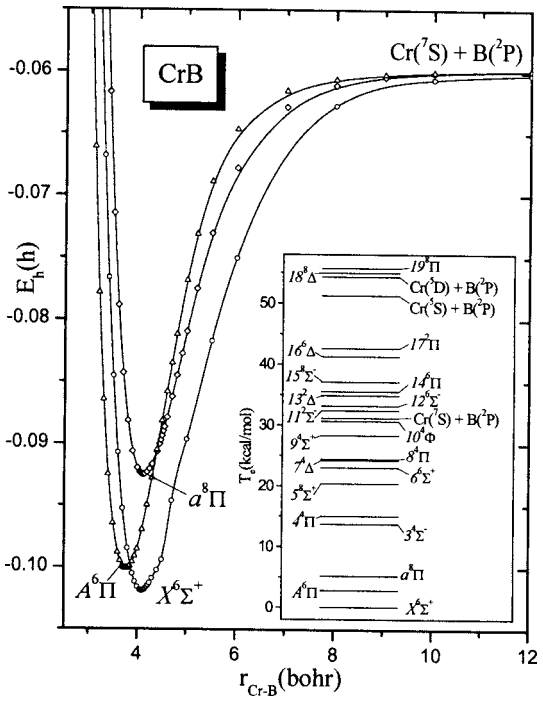

FIG. 4. MRCI/5Z potential energy curves of the CrB molecule. All energies shifted by $+1068.0E_h$. Inset: MRCI+Q/4Z relative energy levels of 20 states of the CrB molecule.

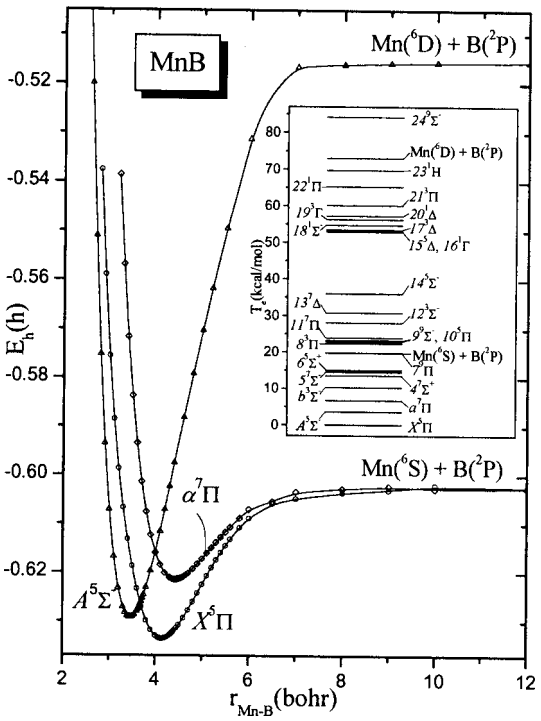

FIG. 5. MRCI/5Z potential energy curves of the MnB molecule. All energies shifted by $+1174.0E_h$. Inset: MRCI+Q/4Z relative energy levels of 25 states of the MnB molecule.

$a\ ^8\Pi$ of 1.995 (2.001) Å, 25.3 (29.1) kcal/mol and 2.182 (2.161) Å, 20.5 (24.5) kcal/mol, respectively, at the MRCI (+Q)/5Z level of theory.

The leading CFs, Mulliken populations, and vbL diagrams describing the bonding scheme of these three states are given below,

$$|X\ ^6\Sigma^+\rangle_{A_1} \approx 0.89|1\sigma^2 2\sigma^2 3\sigma^1 1\pi_x^1 1\pi_y^1 1\delta_+^1 1\delta_-^1\rangle,$$

$$4s^{0.99}4p_z^{0.17}3d_{z^2}^{0.97}3d_{xz}^{0.87}4p_x^{0.01}3d_{yz}^{0.87}4p_y^{0.01}3d_{x^2-y^2}^{1.00}3d_{xy}^{1.00}/$$
$$2s^{1.73}2p_z^{1.01}2p_x^{0.15}2p_y^{0.15},$$

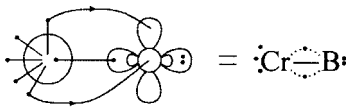

$$|A\ ^6\Pi\rangle_{B_1} \approx |1\sigma^2 2\sigma^1 3\sigma^1[0.79(1\pi_x^2 1\pi_y^1) + 0.30(1\pi_x^1 2\bar{\pi}_x^1 1\pi_y^1) - 0.25(2\pi_x^2 1\pi_y^1)]1\delta_+^1 1\delta_-^1\rangle,$$

$$4s^{0.92}4p_z^{0.19}3d_{z^2}^{0.84}3d_{xz}^{0.95}4p_x^{0.02}3d_{yz}^{0.95}4p_y^{0.02}3d_{x^2-y^2}^{1.00}3d_{xy}^{1.00}/$$
$$2s^{1.53}2p_z^{0.48}2p_x^{0.53}2p_y^{0.53},$$

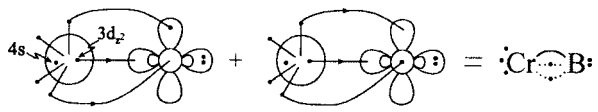

$$|a\ ^8\Pi\rangle_{B_1} \approx 0.97|1\sigma^2 2\sigma^1 3\sigma^1 1\pi_x^1 2\pi_x^1 1\pi_y^1 1\delta_+^1 1\delta_-^1\rangle,$$

$$4s^{0.70}4p_z^{0.05}3d_{z^2}^{0.95}3d_{xz}^{0.99}4p_x^{0.02}3d_{yz}^{0.99}4p_y^{0.02}3d_{x^2-y^2}^{1.00}3d_{xy}^{1.00}/$$
$$2s^{1.72}2p_z^{0.53}2p_x^{0.51}2p_y^{0.51}.$$

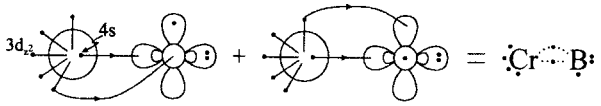

The bonding in the $X\ ^6\Sigma^+$ state can be described as $(\sigma, \frac{1}{2}\pi, \frac{1}{2}\pi)$, that in $A\ ^6\Pi$ as $(\frac{1}{2}\sigma, \pi, \frac{1}{2}\pi)$, and that in $a\ ^8\Pi$ as $(\frac{1}{2}\sigma, \frac{1}{2}\pi)$. Notice that according to the atomic populations the π bonds in all three states are rather weak, but particularly so in the $a\ ^8\Pi$ state where less than $0.05e^-$ are transferred from Cr to B along the π frame.

In the inset of Fig. 4, the relative energy ordering of 20 states of CrB is depicted. The third and fourth excited states are of $^4\Sigma^-$ and $^4\Pi$ symmetries lying 12 and 13 kcal/mol above the ground state at the MRCI/5Z level of theory.

Contrasting the neutral CrB molecule with the CrB^+ cation,[5(d)] we observe that the $X\ ^7\Sigma^+$ state of CrB^+ results from the $X\ ^6\Sigma^+$ of CrB by removing the $4s^1$ electron. The D_e values of the two species are similar, however, in the $X\ ^7\Sigma^+$ state of CrB^+, the r_e value is larger than that of $X\ ^6\Sigma^+$ (CrB) by 0.05 Å.

E. MnB

In Fig. 5, three MRCI/5Z PECs of MnB are displayed with an inset displaying the relative energies of 25 MRCI

+Q/4Z states. The ground state is clearly of $^5\Pi$ symmetry correlating to the ground state fragments $Mn(a\,^6S;s^2d^5)+B(^2P)$; to the ground state fragment dissociates as well the second excited state $a\,^7\Pi$. The first excited state $A\,^5\Sigma^-$ correlates smoothly to the first excited state of $Mn(a\,^6D;4s^13d^6)$, experimentally 2.14 eV above the $a\,^6S$ state.[13] All three states maintain their character up to equilibrium. The main CASSCF CFs, Mulliken distributions, and bonding schemes of these three states are presented below,

$$|X\,^5\Pi\rangle_{B_1} \approx |1\sigma^2 2\sigma^2 3\sigma^1[0.64(1\pi_x^1 2\bar{\pi}_x^1) + 0.39(1\pi_x^2)]1\pi_y^1 1\delta_+^1 1\delta_-^1\rangle - |[0.28(1\sigma^2 3\sigma^1 4\sigma^2) + 0.20(1\sigma^2 2\sigma^1 3\bar{\sigma}^1 4\sigma^1)] \times 1\pi_x^1 2\bar{\pi}_x^1 1\pi_y^1 1\delta_+^1 1\delta_-^1\rangle,$$

$$4s^{1.13}4p_z^{0.35}3d_{z^2}^{1.04}3d_{xz}^{1.03}4p_x^{0.02}3d_{yz}^{1.03}4p_y^{0.02}3d_{x^2-y^2}^{1.00}3d_{xy}^{1.00}/ 2s^{1.69}2p_z^{0.75}2p_x^{0.47}2p_y^{0.47},$$

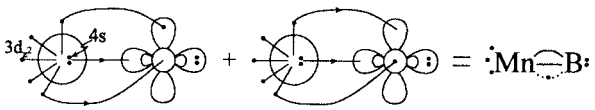

$$|A\,^5\Sigma^-\rangle_{A_2} \approx |1\sigma^2 2\sigma^1 3\sigma^1[0.65(1\pi_x^2 1\pi_y^2) - 0.25(1\pi_x^2 2\pi_y^2 + 2\pi_x^2 1\pi_y^2)]1\delta_+^1 1\delta_-^1\rangle = |A_2\rangle,$$

$$4s^{0.99}4p_z^{0.29}3d_{z^2}^{1.01}3d_{xz}^{1.18}4p_x^{0.04}3d_{yz}^{1.18}4p_y^{0.04}3d_{x^2-y^2}^{1.00}3d_{xy}^{1.00}/ 2s^{1.44}2p_z^{0.26}2p_x^{0.75}2p_y^{0.75},$$

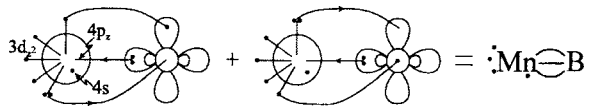

$$|a\,^7\Pi\rangle_{B_1} \approx |[0.77(1\sigma^2 2\sigma^2 3\sigma^1 1\pi_x^1 2\pi_x^1) + 0.35(1\sigma^2 2\sigma^1 3\sigma^1 4\sigma^1 1\pi_x^1 2\bar{\pi}_x^1) - 0.28(1\sigma^2 3\sigma^1 4\sigma^2 1\pi_x^1 2\pi_x^1)]1\pi_y^1 1\delta_+^1 1\delta_-^1\rangle,$$

$$4s^{1.14}4p_z^{0.35}3d_{z^2}^{1.03}3d_{xz}^{1.01}4p_x^{0.03}3d_{yz}^{1.01}4p_y^{0.03}3d_{x^2-y^2}^{1.00}3d_{xy}^{1.00}/ 2s^{1.70}2p_z^{0.73}2p_x^{0.48}2p_y^{0.48}.$$

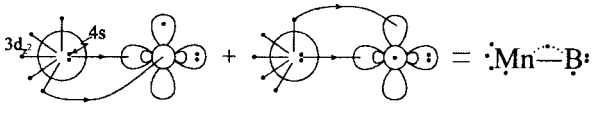

According to the diagrams above, the bonding in the $X\,^5\Pi$ state can be attributed to a $(\sigma,\pi,\frac{1}{2}\pi)$ scheme that in $A\,^5\Sigma^-$ to a genuine triple bond (σ,π,π), and that in the $a\,^7\Pi$ state to a $(\sigma,\frac{1}{2}\pi)$ bond character. Note the very large D_e value and short interatomic distance of the $A\,^5\Sigma^-$ state [71.4 (72.2) kcal/mol, 1.832 (1.832) Å] as contrasted to $X\,^5\Pi$ [19.5 (19.7) kcal/mol, 2.190 (2.183) Å] and to $a\,^7\Pi$ [11.9 (12.2) kcal/mol, 2.343 (2.357) Å] states at the MRCI (+Q)/5Z level.

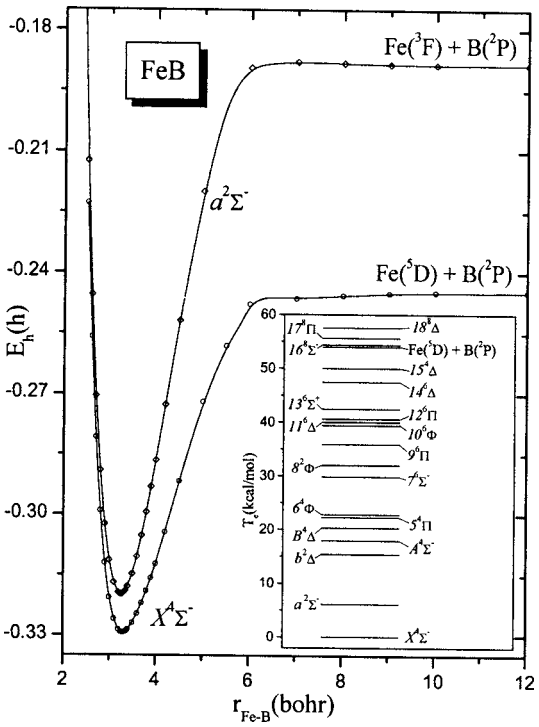

FIG. 6. MRCI/5Z potential energy curves of the FeB molecule. All energies shifted by $+1287.0E_h$. Inset: MRCI+Q/4Z relative energy levels of 19 states of the FeB molecule.

The inset of Fig. 5 shows the relative energy ordering of 25 states of MnB. The third excited state, $b\,^3\Sigma^-$, is situated 11.0 and 3.4 kcal/mol above the ground and the second excited state, respectively, at the MRCI/5Z level of theory.

F. FeB

The MRCI/5Z potential energy curves of the $X\,^4\Sigma^-$ and $a\,^2\Sigma^-$ states of FeB are displayed in Fig. 6; the inset shows relative energies of 19 states of FeB at the MRCI+Q/4Z level of theory. Leading equilibrium CASSCF CFs, atomic populations, and the first three σ molecular orbitals of the first two Σ^- states are as follows:

$$|X\,^4\Sigma^-\rangle_{A_2} \approx 0.82|1\sigma^2 2\sigma^2 3\sigma^1 1\pi_x^2 1\pi_y^2 1\delta_+^1 1\delta_-^1\rangle,$$

$$4s^{1.03}4p_z^{0.44}3d_{z^2}^{1.50}3d_{xz}^{1.49}4p_x^{0.02}3d_{yz}^{1.49}4p_y^{0.02}3d_{x^2-y^2}^{1.00}3d_{xy}^{1.00}/ 2s^{1.48}2p_z^{0.53}2p_x^{0.46}2p_y^{0.46},$$

$$1\sigma \approx 0.90(2s)_B + 0.29(4s)_{Fe},$$

$$2\sigma \approx 0.83(3d_{z^2})_{Fe} - 0.52(2p_z)_B,$$

$$3\sigma \approx 0.85(4s)_{Fe} - 0.46(4p_z)_{Fe} - 0.27(3d_{z^2})_{Fe} - 0.21(2s)_B,$$

$$|a\,^2\Sigma^-\rangle_{A_2} \approx 0.70|1\sigma^2 2\sigma^2 3\sigma^1 1\pi_x^2 1\pi_y^2 1\bar{\delta}_+^1 1\delta_-^1\rangle + 0.40|1\sigma^2 2\sigma^2 3\sigma^1 1\pi_x^2 1\pi_y^2 1\delta_+^1 1\bar{\delta}_-^1\rangle,$$

$$4s^{1.21}4p_z^{0.29}3d_{z^2}^{1.59}3d_{xz}^{1.45}4p_x^{0.03}3d_{yz}^{1.45}4p_y^{0.03}3d_{x^2-y^2}^{1.00}3d_{xy}^{1.00}/$$
$$2s^{1.35}2p_z^{0.53}2p_x^{0.50}2p_y^{0.50},$$

$$1\sigma \approx 0.85(2s)_B + 0.44(4s)_{Fe},$$

$$2\sigma \approx 0.87(3d_{z^2})_{Fe} - 0.40(2p_z)_B - 0.25(4s)_{Fe},$$

$$3\sigma \approx 0.77(4s)_{Fe} - 0.45(2p_z)_B - 0.42(2s)_B - 0.30(4p_z)_{Fe}.$$

It is clear that for both states the 1σ is mainly the $2s$ boron atomic orbital, the 3σ is the $4s$ Fe orbital, and the 2σ represents a bonding interaction between the $3d_{z^2}$ on Fe and $2p_z$ on B.

The $X\,^4\Sigma^-$ correlates adiabatically to the ground state fragments $Fe(a\,^5D;4s^2 3d^6)+B(^2P)$. However, its interaction with a $^4\Sigma^-$ state emanating from the first excited state of Fe, $a\,^5F(4s^1 3d^7)$ 0.875 eV higher,[13] changes its character, thus explaining the singly occupied $4s$ Fe orbital at equilibrium (see populations above). The $a\,^2\Sigma^-$ state correlates to the second excited state of Fe, $a\,^3F(4s^1 3d^7)$ experimentally 1.488 eV above the $a\,^5D$ state[13] (see Fig. 6).

A bonding diagram for both states and consistent with the above discussion is the following, suggesting a triple (σ,π,π) bond.

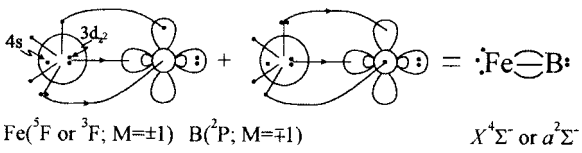

With respect to the ground state fragments, the MRCI (+Q)/5Z binding energy of the $X\,^4\Sigma^-$ state is D_e=53.1 (54.1) kcal/mol, but 74.6 (76.7) kcal/mol diabatically, i.e., with respect to the ^5F state of Fe, at r_e=1.743 (1.747) Å. The corresponding values for the $a\,^2\Sigma^-$ are D_e=82.4 (83.8) kcal/mol at r_e=1.725 (1.726) Å (Table II). Having identical bonding characters, the r_e values of the two states are similar, as expected, whereas the *diabatic* D_e of the $X\,^4\Sigma^-$ state and the D_e of the $a\,^2\Sigma^-$ state differ by about 7 kcal/mol. The second and third excited states, $b\,^2\Delta$ and $A\,^4\Sigma^-$, are located 15.4 and 17.9 kcal/mol higher at the MRCI+Q/4Z level of theory.

G. CoB

Figure 7 shows the MRCI/5Z PECs of the $X\,^3\Delta$ and $a\,^1\Delta$ states of CoB, their energy difference being 3.29 (2.86) kcal/mol. The dominant CASSCF equilibrium CFs, total atomic Mulliken populations, and a vbL diagram (common for both states) are given below,

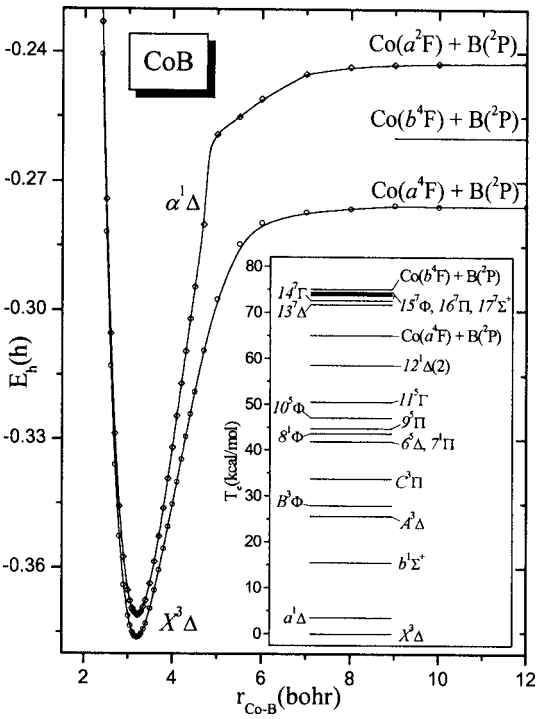

FIG. 7. MRCI/5Z potential energy curves of the CoB molecule. All energies shifted by $+1406.0E_h$. Inset: MRCI+Q/4Z relative energy levels of 18 states of the CoB molecule.

$$|X\,^3\Delta\rangle_{A_1+A_2} \approx 0.88\left|\frac{1}{\sqrt{2}}(1\sigma^2 2\sigma^2 3\sigma^1 1\pi_x^2 1\pi_y^2)(1\delta_+^1 1\delta_-^2 + 1\delta_+^2 1\delta_-^1)\right\rangle,$$

$$4s^{1.04}4p_z^{0.37}3d_{z^2}^{1.60}3d_{xz}^{1.51}4p_x^{0.02}3d_{yz}^{1.51}4p_y^{0.02}3d_{x^2-y^2}^{1.50}3d_{xy}^{1.50}/$$
$$2s^{1.47}2p_z^{0.49}2p_x^{0.45}2p_y^{0.45},$$

$$|a\,^1\Delta\rangle_{A_1+A_2} \approx 0.86\left|\frac{1}{\sqrt{2}}(1\sigma^2 2\sigma^2 3\bar{\sigma}^1 1\pi_x^2 1\pi_y^2)(1\delta_+^1 1\delta_-^2 + 1\delta_+^2 1\delta_-^1)\right\rangle,$$

$$4s^{1.14}4p_z^{0.27}3d_{z^2}^{1.65}3d_{xz}^{1.49}4p_x^{0.02}3d_{yz}^{1.49}4p_y^{0.02}3d_{x^2-y^2}^{1.50}3d_{xy}^{1.50}/$$
$$2s^{1.40}2p_z^{0.51}2p_x^{0.46}2p_y^{0.46}.$$

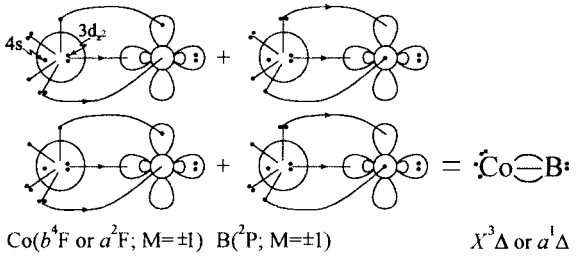

These two Δ states have obviously the same type of bonding; they only differ by a spin flip in the $3\sigma(\approx 4s_{Fe})$ orbital, and they are very similar as well to the previously described $X\,^4\Sigma^-$ and $a\,^2\Sigma^-$ states of FeB, differing from those by an observer d electron irrelevant to the bonding. In an analogous way as in the $X\,^4\Sigma^-$ state of FeB, the $X\,^3\Delta$ interacts

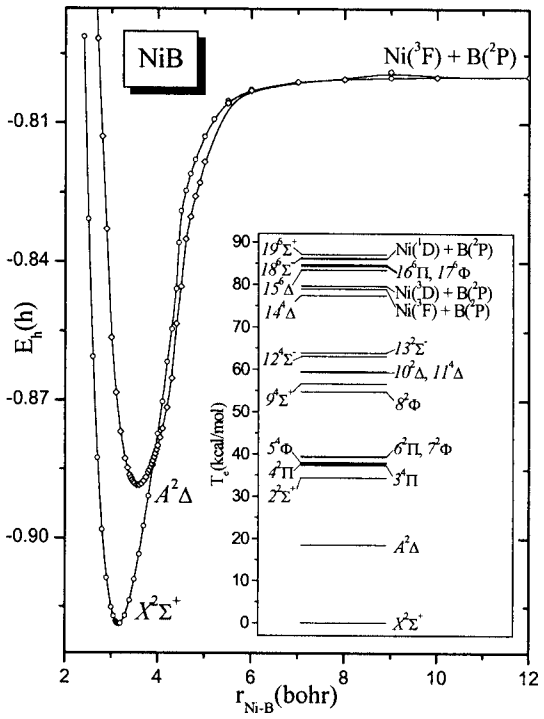

FIG. 8. MRCI/5Z potential energy curves of the NiB molecule. All energies shifted by $+1531.0E_h$. Inset: MRCI+Q/4Z relative energy levels of 20 states of the NiB molecule.

with the first excited state of Co($b\ ^4F;4s^13d^8$) located 0.417 eV above the $a\ ^4F(4s^13d^8)$,[13] thus transferring its character to equilibrium. The $a\ ^2F$ correlates adiabatically to the second excited state of Co($a\ ^2F;4s^13d^8$)+B(^2P) (see Fig. 7). Both $X\ ^3\Delta$ and $a\ ^1\Delta$ states feature a triple (σ,π,π) bond. The binding energy of the $X\ ^3\Delta$ with respect to Co($a\ ^4F$) is D_e=63.1 (65.7) kcal/mol at r_e=1.696 (1.700) Å, but diabatically, i.e., with respect to Co($b\ ^4F;4s^13d^8$), D_e=73.0 (76.1) kcal/mol. Correspondingly, for the $a\ ^1\Delta$ state, D_e =80.7 (83.2) kcal/mol and r_e=1.700 (1.704) Å.

Notice the striking similarity of the diabatic D_e values of the $X\ ^4\Sigma^-$(FeB) and $X\ ^3\Delta$(CoB), 76.7 versus 76.1 kcal/mol; the same holds true for the $a\ ^2\Sigma^-$(FeB) and $a\ ^1\Delta$(CoB), 83.8 versus 83.2 kcal/mol. Their bond distances indicate certainly the same trend.

The inset of Fig. 7 shows the relative energy ordering of 18 states of CoB. The second excited state, $b\ ^1\Sigma^+$, lies 19 (13) kcal/mol above the *X*-state at the MRCI(+Q)/5Z level of theory.

H. NiB

The potential energy curves of the first two lowest states of NiB, $X\ ^2\Sigma^+$ and $A\ ^2\Delta$, are shown in Fig. 8. The ground state of Ni is $a\ ^3F_4(4s^23d^8)$, with a $a\ ^3D_3(4s^13d^9)$ component a mere 0.0254 eV higher. Taking into account the M_J projections, the order is reversed by 0.0298 eV, the $a\ ^3D$ being now the lowest.[13] Clearly, for all practical purposes the $a\ ^3F$ and $a\ ^3D$ terms can be thought as degenerate.

The $A\ ^2\Delta$ state is 19 (17.9) kcal/mol above the *X*-state at the MRCI(+Q)/5Z level. Both states correlate adiabatically to Ni($a\ ^3F$)+B(^2P), but they change character because of an avoided crossing of the $X\ ^2\Sigma^+$ with the $2\ ^2\Sigma^+$ state near 4.2 bohrs, and the $A\ ^2\Delta$ with the $10\ ^2\Delta$ at 4.8 bohrs. Thus, both states correlate diabatically to Ni($a\ ^3D$)+B(^2P).

The CASSCF leading CFs, Mulliken distributions, and vbL diagrams of the *X*- and *A*-states are given below,

$$|X\ ^2\Sigma^+\rangle_{A_1} \approx 0.91|1\sigma^2 2\sigma^2 3\sigma^1 1\pi_x^2 1\pi_y^2 1\delta_+^2 1\delta_-^2\rangle,$$

$$4s^{1.04}4p_z^{0.29}3d_{z^2}^{1.66}3d_{xz}^{1.55}4p_x^{0.02}3d_{yz}^{1.55}4p_y^{0.02}3d_{x^2-y^2}^{1.99}3d_{xy}^{1.99}/$$
$$2s^{1.48}2p_z^{0.50}2p_x^{0.42}2p_y^{0.42},$$

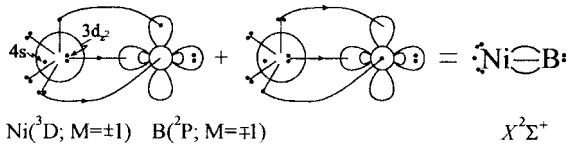

$$|A\ ^2\Delta\rangle_{A_1+A_2}$$
$$\approx 0.96\left|\frac{1}{\sqrt{2}}(1\sigma^2 2\sigma^2 3\sigma^2 1\pi_x^2 1\pi_y^2)(1\delta_+^1 1\delta_-^2 + 1\delta_+^2 1\delta_-^1)\right\rangle,$$

$$4s^{1.29}4p_z^{0.14}3d_{z^2}^{1.78}3d_{xz}^{1.88}4p_x^{0.01}3d_{yz}^{1.88}4p_y^{0.01}3d_{x^2-y^2}^{1.50}3d_{xy}^{1.50}/$$
$$2s^{1.71}2p_z^{1.04}2p_x^{0.10}2p_y^{0.10}.$$

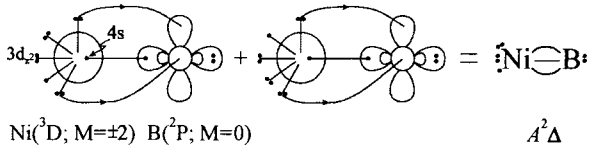

Finally, both states show a triple bond character with binding energies of 74.7 (79.2) and 55.4 (61.2) kcal/mol, with bond distances of 1.676 (1.681) and 1.892 (1.890) Å for the $X\ ^2\Sigma^+$ and $A\ ^2\Delta$ states, respectively. The first excited state has an elongated bond and a smaller D_e value by 0.2 Å and 19 kcal/mol, as compared to the $X\ ^2\Sigma^+$ state.

The inset of Fig. 8 shows the relative energy ordering of 20 states of NiB. The second excited state is $2\ ^2\Sigma^+$ lying 34 kcal/mol above the ground state at the MRCI+Q/4Z level of theory.

I. CuB

Although copper has its $3d$ shell filled ($3d^{10}$), it can be considered as the last first row $3d$ transition metal element because Cu^{II} has a $3d^9$ (^2D) configuration, i.e., a partially filled $3d$ shell. Figure 9 shows the MRCI/5Z PECs of all states which spring of the ground state atoms, Cu(^2S) +B(^2P), namely, $X\ ^1\Sigma^+$, $a\ ^3\Pi$, $B\ ^1\Pi$, and $b\ ^3\Sigma^+$. The PEC of one more state of symmetry $^1\Sigma^+$ is displayed, in essence degenerate to the $a\ ^3\Pi$ and correlating to the first excited state of Cu($^2D;4s^23d^9$) 1.490 eV above the Cu ^2S state.[13] The relative energies of 19 states calculated at the MRCI +Q/5Z level are also shown in the inset of Fig. 9.

With no doubt the ground state of CuB is of symmetry $^1\Sigma^+$, described adequately by a single determinant, $|X\ ^1\Sigma^+\rangle_{A_1} \approx 0.96|1\sigma^2 2\sigma^2 3\sigma^2 1\pi_x^2 1\pi_y^2 1\delta_+^2 1\delta_-^2\rangle$ at the MRCI level. The MRCI Mulliken atomic populations

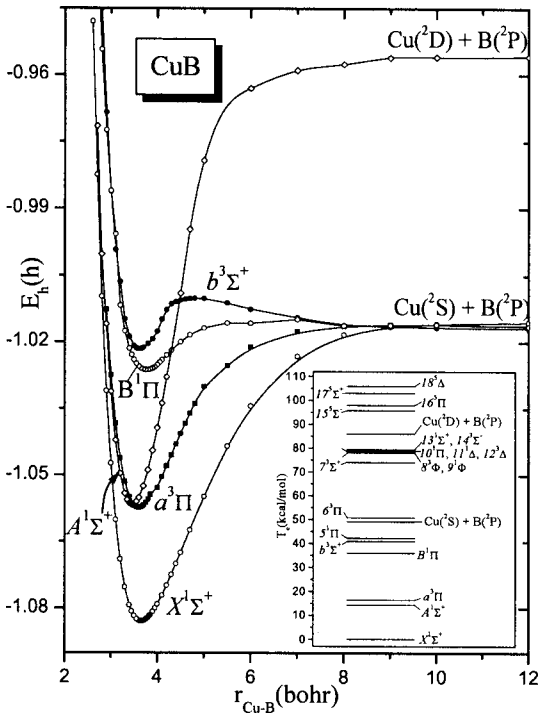

FIG. 9. MRCI/5Z potential energy curves of the CuB molecule. All energies shifted by $+1663.0E_h$. Inset: MRCI+Q/5Z relative energy levels of 19 states of the CuB molecule.

$$4s^{1.18}4p_z^{0.14}3d_{z^2}^{1.87}3d_{xz}^{1.89}4p_x^{0.01}3d_{yz}^{1.89}4p_y^{0.01}3d_{x^2-y^2}^{1.99}3d_{xy}^{1.99}/$$
$$2s^{1.70}2p_z^{0.98}2p_x^{0.12}2p_y^{0.12}$$

point clearly to the following vbL bonding diagram:

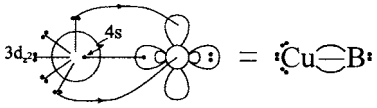

$Cu(^2S)$ $B(^2P; M=0)$ $X^1\Sigma^+$

suggesting a σ and two weak π bonds. The former results from a transfer of about $0.25e^-$ from B to Cu, whereas the latter from a transfer of $0.25e^-$ from Cu to B through the π system. At the MRCI(+Q)/5Z level, D_e=42.4 (49.1) kcal/mol at r_e=1.934 (1.922) Å and μ_{FF}=1.71 (1.62) D. Barysz and Urban,[3] using a $[9s7p3d1f/_{Cu}5s3p2d/_B]$ basis set, performed CASPT2 and CCSD(T) calculations on the $X\ ^1\Sigma^+$ state of CuB. Their results depend very strongly on the method used: For instance, at the CASPT2, CASPT2+quasirelativistic, and CCSD(T)+quasirelativistic corrections, D_e (kcal/mol)=64.7, 54.3, and 35.1 kcal/mol, respectively.

It should be mentioned at this point that the construction of the $X\ ^1\Sigma^+$ potential energy curve of CuB was met with severe difficulties. Small differences in the character of the CASSCF valence orbitals or slight differences in the initial (guess) CAS orbitals resulted in discontinuities in the MRCI PEC, wildly varying configuration state functions MRCI coefficients, and different absolute MRCI energies and, of course, D_e values. However, in all the above cases, the Davidson correction (+Q) seems to improve the D_e value of the MRCI method. The situation was remedied by including three more active orbitals in the reference (CASSCF) function (13 instead of 10 as in all presently studied MBs, M=Sc to Ni), of symmetries $a_1(4p_z)$, $b_1(4d_{xz})$, and $b_2(4d_{yz})$, orbitals of Cu. Now, although the MRCI virtual space was constructed from the natural orbitals of the 13 orbitals CASSCF wave function, the reference function was truncated in such a way as to be equivalent to a ten active orbital CASSCF description. Thus, our final MRCI $X\ ^1\Sigma^+$ expansion is of comparable quality with the MRCI functions of the previously studied MBs, M=Sc to Ni.

Two states are competing for the first excited state of CuB, $a\ ^3\Pi$ and $A\ ^1\Sigma^+$ (see Fig. 9). At the MRCI(+Q)/5Z level, they lie 16.0 (16.4) and 16.5 (14.3) kcal/mol above the $X\ ^1\Sigma^+$ state. The $a\ ^3\Pi$ correlates to the ground state fragments $Cu(a\ ^2S;4s^13d^{10})+B(^2P)$, maintaining this character to equilibrium at r_e=1.904 (1.885) Å. The $A\ ^1\Sigma^+$ state correlates smoothly to the first excited state of Cu, $a\ ^2D$ $(4s^23d^9)$, at r_e=1.830 (1.828) Å and D_e=63.3 (71.7) kcal/mol as contrasted to D_e=25.8 (31.5) kcal/mol of the $a\ ^3\Pi$ state. The most important equilibrium CFs, atomic Mulliken densities, and vbL diagrams of these two states are shown below,

$$|a\ ^3\Pi\rangle_{B_1+B_2} \approx \frac{0.94}{\sqrt{2}}|1\sigma^2 2\sigma^2 3\sigma^1(1\pi_x^2 2\pi_x^1 1\pi_y^2 + 1\pi_x^2 1\pi_y^2 2\pi_y^1)1\delta_+^2 1\delta_-^2\rangle,$$

$$4s^{0.84}4p_z^{0.11}3d_{z^2}^{1.88}3d_{xz}^{1.96}4p_x^{0.05}3d_{yz}^{1.96}4p_y^{0.05}3d_{x^2-y^2}^{1.99}3d_{xy}^{1.99}/$$
$$2s^{1.47}2p_z^{0.64}2p_x^{0.51}2p_y^{0.51},$$

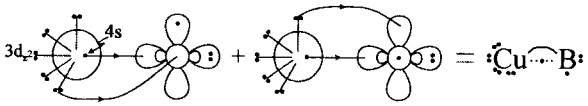

$Cu(^2S)$ $B(^2P; M=\pm1)$ $a^3\Pi$

$$|A\ ^1\Sigma^+\rangle_{A_1} \approx |1\sigma^2 2\sigma^2 3\sigma^2[0.75(1\pi_x^2 1\pi_y^2) + 0.31(1\pi_x^1 2\bar{\pi}_x^1 1\pi_y^2 + 1\pi_x^2 1\pi_y^1 2\bar{\pi}_y^1)]1\delta_+^2 1\delta_-^2\rangle,$$

$$4s^{1.32}4p_z^{0.33}3d_{z^2}^{1.90}3d_{xz}^{1.72}4p_x^{0.02}3d_{yz}^{1.72}4p_y^{0.02}3d_{x^2-y^2}^{1.99}3d_{xy}^{1.99}/$$
$$2s^{1.57}2p_z^{0.77}2p_x^{0.27}2p_y^{0.27}.$$

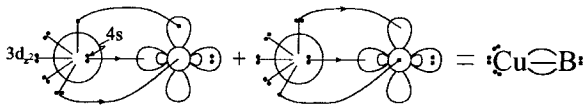

$Cu(^2D; M=\pm1)$ $B(^2P; M=\mp1)$ $A^1\Sigma^+$

The attractive interaction in the $a\ ^3\Pi$ state can be ascribed to a π and a $\frac{1}{2}\sigma$ bond, where $0.2e^-$ are transferred mainly through the σ frame to the B atom, whereas in the $A\ ^1\Sigma^+$ we have a triple bond (σ,π,π), where $0.4e^-$ are transferred through the σ frame to the B atom and about $0.4e^-$ are backdonated through the π frame.

The third and fourth excited states, $B\ ^1\Pi$ and $b\ ^3\Sigma^+$, lie 35.5 (36.0) and 38.5 (40.9) kcal/mol above the $X\ ^1\Sigma^+$ state at the MRCI(+Q)/5Z level of theory, and both correlate smoothly to the ground state fragments $Cu(a\ ^2S)+B(^2P)$ (Fig. 9). They are weakly bound with D_e=6.2 (11.9) and 2.9

(6.9) kcal/mol at r_e=1.995 (1.936) and 1.912 (1.933) Å for $B\ ^1\Pi$ and $b\ ^3\Sigma^+$, respectively. The MRCI main CFs and Mulliken population analysis of the two states and vbL icon of the $b\ ^3\Sigma^+$ state are given below (the vbL icon of $A\ ^1\Pi$ is the same with that of $A\ ^3\Pi$; the two states differ only in spin multiplicity),

$$|B\ ^1\Pi\rangle_{B_1+B_2} \approx \frac{0.93}{\sqrt{2}}|1\sigma^2 2\sigma^2 3\sigma^1(1\pi_x^2 2\bar{\pi}_x^1 1\pi_y^2 + 1\pi_x^2 1\pi_y^2 2\bar{\pi}_y^1)1\delta_+^2 1\delta_-^2\rangle,$$

$$4s^{0.77}4p_z^{0.10}3d_{z^2}^{1.93}3d_{xz}^{1.97}4p_x^{0.02}3d_{yz}^{1.97}4p_y^{0.02}3d_{x^2-y^2}^{1.99}3d_{xy}^{1.99}/2s^{1.67}2p_z^{0.46}2p_x^{0.52}2p_y^{0.52},$$

$$|b\ ^3\Sigma^+\rangle_{A_1} \approx 0.93|1\sigma^2 2\sigma^2 3\sigma^1 4\sigma^1 1\pi_x^2 1\pi_y^2 1\delta_+^2 1\delta_-^2\rangle,$$

$$4s^{1.01}4p_z^{0.54}3d_{z^2}^{1.94}3d_{xz}^{1.80}4p_x^{0.02}3d_{yz}^{1.80}4p_y^{0.02}3d_{x^2-y^2}^{1.99}3d_{xy}^{1.99}/2s^{1.59}2p_z^{0.84}2p_x^{0.18}2p_y^{0.18}.$$

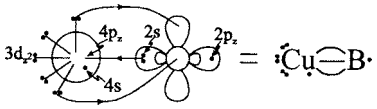

The inset of Fig. 9 shows the MRCI/5Z relative energy ordering of 19 states of CuB. The fifth excited state, $5\ ^1\Pi$, lies 42.3 kcal/mol above the ground state MRCI/5Z level of theory.

IV. SUMMARY AND FINAL REMARKS

At the multireference CASSCF+1+2 (=MRCI) level and in conjunction with quintuple ([9*s*8*p*6*d*4*f*3*g*2*h*1*i*/$_M$ 6*s*5*p*4*d*3*f*2*g*1*h*/$_B$]=5Z) correlation consistent basis sets, we have examined the electronic structure and bonding of the nine diatomic borides, MB, M=Sc to Cu. For the lowest two to five states for each MB species we have constructed full potential energy curves, while at the MRCI+Q/4Z level we have calculated relative energies for about 20 states for every MB molecule. At the MRCI/5Z level, we report total energies, dissociation energies, dipole moments, and common spectroscopic parameters. It should be stressed that experimental results on the 3*d* metal borides are completely lacking, whereas only two theoretical structural works, one on ScB (Ref. 4) and one on the ground state of CuB, (Ref. 3) have been reported so far in the literature.

In what follows, some general remarks are made and we also give a summary of our main conclusions.

(i) Table III lists the ground states of the MBs along with "recommended" bond distances, dissociation energies, and dipole moments. The r_e values of ScB($X\ ^5\Sigma^-$) and TiB($X\ ^6\Delta$), which have been also obtained at a highest level of theory, C-MRCI+DKH2+Q/cc-pwCV5Z, are 0.04 and 0.03 Å shorter than those of the plain MRCI/5Z values. The VB to CuB r_e's of Table III are MRCI+Q/5Z values reduced by 0.02 Å and rounded to the second decimal point. Recommended D_e's are simply MRCI+Q/5Z values rounded to the closest integer number. The D_e results of Table III are represented graphically in Fig. 10. Observe that the dissociation energies follow a V-shaped curve, with the MnB on the apex having the lowest D_e(=20 kcal/mol). With respect to the diabatic end fragments, FeB($X\ ^4\Sigma^-$), CoB($X\ ^3\Delta$), and NiB($X\ ^2\Sigma^+$) have D_e values of 77, 76, and 79 kcal/mol, respectively, and very similar bonding and bond distances.

(ii) With the exception of the CrB and CuB molecules, the *in situ* B atom in the ground states of the remaining seven borides is in the M=±1 component of the ^2P state; in the *X*-states of CrB and CuB, M=0.

(iii) With the exception of MnB where the *in situ* metal has a $4s^2 3d^q$ configuration in the $X\ ^5\Pi$ state, the metal in the *X*-states of the eight MB species has a $4s^1 3d^{q+1}$ distribution.

(iv) In the ground state of most of the MB species, there is a weak Mulliken charge transfer of $0.1e^-$ to $0.2e^-$ from M to B. This tendency seems to be reversed in CoB and NiB, where about $0.1e^-$ are transferred from B to Co or Ni, whereas in MnB($X\ ^5\Pi$) about $0.4e^-$ move from Mn to B.

TABLE III. Recommended bond distances r_e (Å), dissociation energies D_e (kcal/mol), and dipole moments μ (D) of the ground states of the MB molecules, M=Sc to Cu.

Species	State	r_e	D_e	μ[a]
ScB	$^5\Sigma^-$	2.09[b]	76	4.0[c]
TiB	$^6\Delta$	2.05[b]	65	3.3[c]
VB	$^7\Sigma^-$	2.02	55	3.2
CrB	$^6\Sigma^+$	2.16	31	2.1
MnB	$^5\Pi$	2.16	20	2.4
FeB	$^4\Sigma^-$	1.73	54	2.1
CoB	$^3\Delta$	1.68	66	1.9
NiB	$^2\Sigma^+$	1.66	79	2.2
CuB	$^1\Sigma^+$	1.90	49	1.7

[a]Rounded finite field dipole moments, μ_{FF}.
[b]C-MRCI+DKH2+Q/cc-pwCV5Z results (see text).
[c]C-MRCI+DKH2/cc-pwCV5Z results.

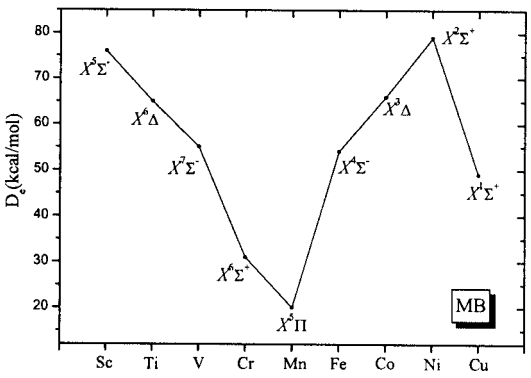

FIG. 10. MRCI+Q/5Z dissociation energies of the ground states of the metal boride MBs, M=Sc to Cu.

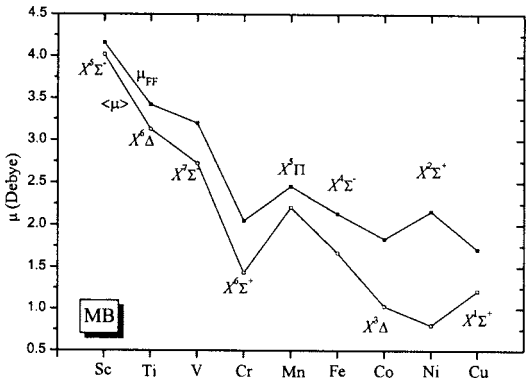

FIG. 11. Finite field (μ_{FF}) and expectation value ($\langle\mu\rangle$) dipole moments of the ground state MBs at the MRCI/5Z level.

(v) Recommended dipole moments of the ground states are also given in Table III. These are finite-field (μ_{FF}) MRCI/5Z values rounded to the first decimal place; the ScB and TiB μ_{FF} values are given at the C-MRCI+DKH2/cc-pwCV5Z level. The general trend of the dipole moments is to become smaller as we move from ScB (μ_{FF}=4.0 D) to CuB(μ_{FF} =1.7 D). Moreover, μ_{FF} and expectation value ones ($\langle\mu\rangle$) are plotted for the nine ground states in Fig. 11. Both μ_{FF} and $\langle\mu\rangle$ follow the same trend, and they are closer for ScB; in general, as we move to the right, their differences increase and their values decrease, with the exception in MnB and CuB. The $\langle\mu\rangle$ values are smaller than the μ_{FF} ones, as in most cases studied in this laboratory.

(vi) The exceptional ability of the boron atom to participate in a variety of bonding schemes is well known. In the present study, the bonding in the MB series varies from three half bonds $(\frac{1}{2}\sigma, \frac{1}{2}\pi, \frac{1}{2}\pi)$ to full triple bonds (σ, π, π), with the realization of all intermediate schemes.

(vii) Many electronic states are very close packed, making the determination of their exact order virtually impossible.

(viii) Finally, we would like to say that we hope that our results will be proven useful, particularly to the experimentalists and to stress that although these are, "chemically" speaking, very simple molecules their theoretical confrontation is far from being routine.

ACKNOWLEDGMENTS

This project is cofunded by the European Social Fund and National Resources via the (EPEAEK II) PYTHAGORAS Grant No. (70/3/7373) program of the Greek Ministry of Education.

[1] N. N. Greenwood and A. Earnshaw, *Chemistry of the Elements*, 2nd ed. (Butterworth-Heinemann, Oxford, 1998).
[2] See experimental values in *CRC Handbook of Chemistry and Physics*, 83rd ed. (CRS press, Boca Raton, 2002). Quoting as source V. N. Kondratiev, *Bond Dissociation Energies, Ionization Potentials and Electron Affinities* (Nauka, Moscow, 1974), which most likely is actually drawing information from K. A. Gingerich, High. Temp. Sci. **1**, 258 (1969), the title of which refers to predicted dissociation energies as mentioned in http://diref.uwaterloo.ca
[3] M. Barysz and M. Urban, Adv. Quantum Chem. **28**, 257 (1997).
[4] I. Černušák, M. Dallos, H. Lischka, T. Müller, and M. Uhlár, J. Chem. Phys. **126**, 214311 (2007).
[5] (a) A. Kalemos and A. Mavridis, Adv. Quantum Chem. **32**, 69 (1998); (b) J. Phys. Chem. A **102**, 5982 (1998); (c) **103**, 3336 (1999); (d) J. Chem. Phys. **113**, 2270 (2000).
[6] See, for example, D. Tzeli and A. Mavridis, J. Chem. Phys. **126**, 194304 (2007), and reference therein.
[7] C. W. Bauschlicher, Jr., Theor. Chim. Acta **92**, 183 (1995).
[8] T. H. Dunning, Jr., J. Chem. Phys. **90**, 1007 (1989).
[9] N. B. Balabanov and K. A. Peterson, J. Chem. Phys. **123**, 064107 (2005).
[10] H.-J. Werner and P. J. Knowles, J. Chem. Phys. **89**, 5803 (1988); P. J. Knowles and H.-J. Werner, Chem. Phys. Lett. **145**, 514 (1988); H.-J. Werner and E. A. Reinsch, J. Chem. Phys. **76**, 3144 (1982); H.-J. Werner, Adv. Chem. Phys. **69**, 1 (1987).
[11] S. R. Langhoff and E. R. Davidson, Int. J. Quantum Chem. **8**, 61 (1974); M. R. A. Blomberg and P. E. M. Sieghbahm, J. Chem. Phys. **78**, 5682 (1983).
[12] H.-J. Werner, P. J. Knowles, R. D. Amos *et al.*, MOLPRO 2002, a package of *ab initio* programs.
[13] C. E. Moore, *Atomic Energy Levels*, NSRDS-NBS Circular No. 35, Washington, D.C. (1971).
[14] M. Douglas and N. M. Kroll, Ann. Phys. (N.Y.) **82**, 89 (1974); B. A. Hess, Phys. Rev. A **32**, 756 (1985); **33**, 3742 (1986); G. Jansen and B. A. Hess, *ibid.* **39**, 6016 (1989).